Journal of Materials Chemistry A

Accepted Manuscript

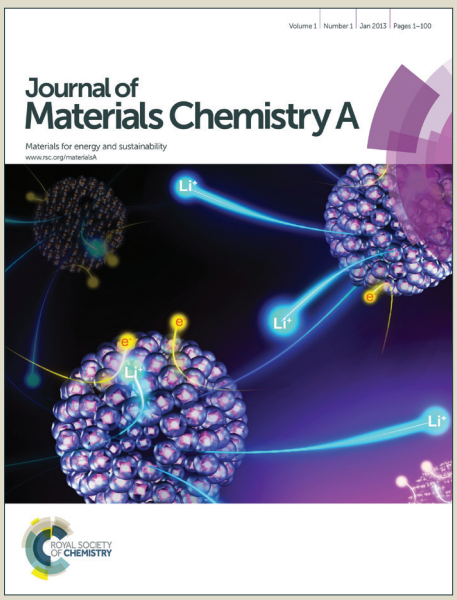

ROYAL SOCIETY OF CHEMISTRY

www.rsc.org/materialsA

Ag@SiO_2–OT NPs well-dispersed in P3HT:PCBM increased the light-harvesting ability and inhibited charge carrier trap to improve photovoltaic performance.

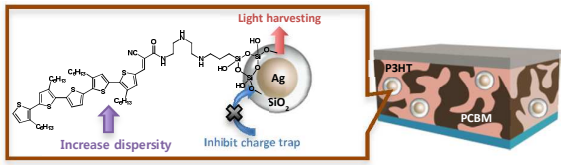

Journal Name

RSCPublishing

ARTICLE

Oligothiophene-Modified Silver/Silica Core-Shell Nanoparticles for Inhibiting Open-Circuit Voltage Drop and Aggregation in Polymer Solar Cells

Cite this: DOI: 10.1039/x0xx00000x

Received ooth January 2012,
Accepted ooth January 2012

DOI: 10.1039/x0xx00000x

www.rsc.org/

Woochul Lee,‡ Joohyun Lim,‡ Jin-Kyu Lee,* and Jong-In Hong*

‡These authors contributed equally

Metal nanoparticles (NPs) have attracted much attention owing to their particular characteristics such as localized surface plasmon resonance (LSPR) and scattering properties, which can improve light-harvesting ability of photovoltaic cells. However, modification of the metal NP surface is needed to prevent particle aggregation and photoinduced charge trapping. Surface modification of silica-coated Ag NPs with oligothiophene (OT) provides silver/silica core-shell ($Ag@SiO_2$−OT) NPs, which are well dispersed in nonpolar organic solvents and miscible with the bulk-heterojunction (BHJ) layer of poly(3-hexylthiophene) (P3HT) and phenyl-C61-butyric acid methyl ester (PCBM) (P3HT:PCBM). Incorporation of the $Ag@SiO_2$−OT NPs into the P3HT:PCBM layers as the active layer of photovoltaic devices improves the light-harvesting ability and enhances the photo-conversion efficiency (PCE) in about 18%. There is no significant change in the open-circuit voltage (V_{oc}) value even when up to 30 wt% of $Ag@SiO_2$−OT NPs are incorporated, confirming that the OT-modified silica layer on silver NPs contributes to improving light absorption and photo-current without causing aggregation and photo-induced charge trapping. Moreover, the deliberately designed transmission electron microscopy (TEM) investigation of the composite films of P3HT:PCBM and $Ag@SiO_2$−OT NPs reveals that $Ag@SiO_2$−OT NPs are mainly located in the P3HT domain owing to the favorable interaction between the similar molecular structures of OT and P3HT.

1. Introduction

Because of the rapid depletion of fossil-fuel energy resources, photovoltaic cells have started to gain recognition as a potential alternative to conventional energy sources with the added benefit of environmental friendliness. Organic photovoltaic cells (OPVs) based on π-conjugated polymers and fullerene derivatives have attracted considerable attention owing to low cost, large-scale fabrication, lightweight, possible solution processing, and mechanical flexibility of the devices.[1] Many efforts have been made toward the development of low band-gap polymers for fabricating high power conversion efficiency (PCE) solar cells.[2, 3] Consequently, the maximum PCE achieved recently exceeded 7%.[4, 5] However, the current PCE values are still low; in order to achieve mass production and practical applications, the device performance needs to be improved to attain a PCE of 10–15%.[6] To attain high efficiency, polymer-based solar cells should fulfil several requirements such as efficient light-harvesting ability and excellent charge carrier separation and charge transport.[2] In general, the photoactive layer should be thick enough to sufficiently absorb the incident light; however, the organic active layer is intrinsically very thin because of the short diffusion length and low carrier mobility of most polymeric materials.[7]

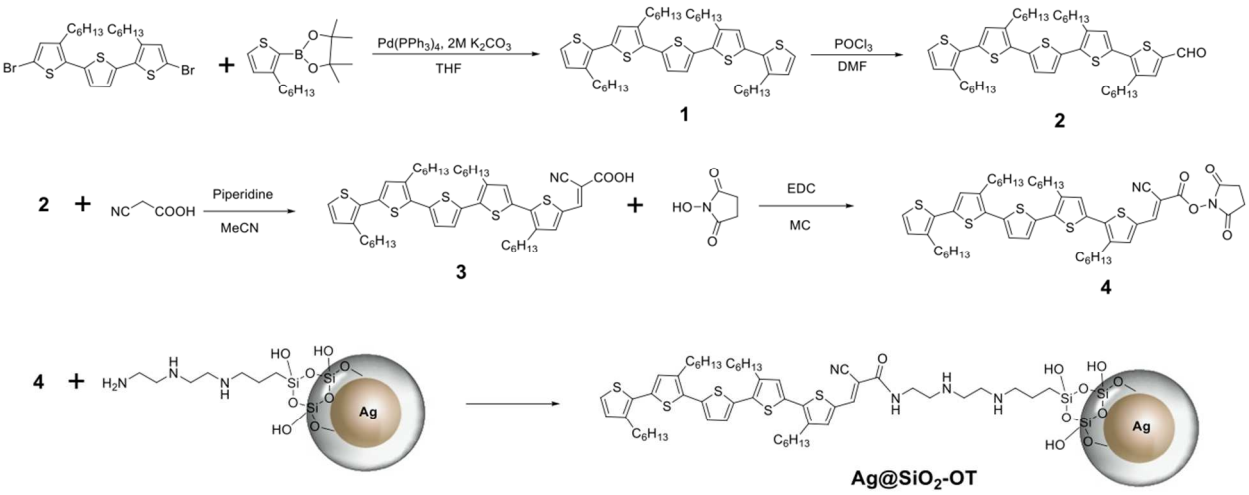

Scheme 1. Synthetic routes for oligothiophene derivatives and surface-modified Ag NPs.

Thus, achieving efficient light trapping in the active layer of polymer-based solar cells is challenging without increasing the film thickness.

Ag and Au nanoparticles (NPs) have extraordinary characteristics such as light-scattering effects and localized surface plasmon resonance (LSPR).[8] These properties are expected to improve the efficiency of solar cells, and two major mechanisms have been proposed.[9] First, the light-scattering effect from small metal NPs increases the optical path length of light, which makes the active layer absorb the incident solar light more efficiently. Second, the LSPR of metal NPs induces the strong local electromagnetic fields around the NPs to increase the light absorption of organic materials. Several groups have reported that metal NPs increased the performance of bulk-heterojunction (BHJ) solar cells without changing the thickness of the active layer.[10-13] However, metal NPs prepared by a typical reduction process in a water or polyol solution are not well dispersed in nonpolar organic solvents.[14,15] Therefore, they cannot be embedded in the active layer (typically composed of P3HT and PCBM);[16-18] they tend to aggregate during the film casting of the active layer owing to their insufficient solubility in both chlorobenzene (CB) and *o*-dichlorobenzene (DCB) and generate defects in the entire cell structure.[19] Due to their solubility and miscibility problem, metal NPs are usually introduced into the hole injection layer with poly(3,4-ethylenedioxythiophene):poly(styrene sulfonate) (PEDOT:PSS), which is water-soluble.[20-22] The NPs prepared using long alkyl chain surfactants, showing good dispersion in nonpolar organic solvents, were expected to prevent aggregation during the coating process.[11] However, the metal NPs still tend to aggregate probably due to the miscibility problem with P3HT-PCBM. A direct contact of the metal NPs with organic electron donor and/or acceptor molecules causes another problem; it can act as a center of photoinduced exciton quenching, and recently, this charge trapping mechanism in the active layer has been reported.[23-25] These electron loss mechanisms and direct contact with the metal cathode reduce the open-circuit voltage (V_{oc}) with increasing concentration of metal NPs.[26] To prevent the exciton quenching on the surface of metal NPs, several groups recently introduced an insulating silica layer onto the surface of metal NPs.[27-29]

In this paper, we prepared a polymer-based BHJ solar cell with the oligothiophene (OT)-modified silica-coated silver NPs (Ag@SiO_2−OT NPs) as an additive to enhance the photocurrent without the drop in V_{oc}. The silica coating on the Ag NPs plays the role of an insulator to prevent direct contact with other organic molecules in the active layer, as well as the role to provide the modification platform based on the well-known silicon chemistry. When the surface of silver/silica core-shell (Ag@SiO_2) NPs is modified with the OT, as expected, the NPs become sufficiently soluble in nonpolar organic solvents and achieve good dispersion in the active layer. Optimizing the amount of the OT-modified silver/silica core-shell NPs (Ag@SiO_2−OT) embedded in a blend of P3HT and PCBM resulted in approximately 18% enhancement of PCE (4.25 %) compared to that of the P3HT:PCBM reference cell (3.59 %) under the same conditions. There was no change in the V_{oc} even after the addition of 30 wt% of Ag@SiO_2−OT NPs in the active layer, while there was a large drop in V_{oc} as a function of the amount of introduced NPs for devices prepared with bare Ag NPs. The location of Ag@SiO_2−OT NPs was precisely investigated by deliberately designed TEM analyses. The cross sectioned TEM images of the Ag@SiO_2−OT NPs embedded in P3HT-PCBM layer revealed that the NPs were distributed in the middle of the active layer, and most of them were mainly found in the P3HT region owing to the favorable interaction between the similar molecular structures of OT and P3HT.

2. Results and discussion

2.1 Synthesis of Ag@SiO_2−OT NPs.

Ag NPs were synthesized by reducing silver nitrate in hot ethylene glycol (EG) in the presence of an excess amount of polyvinylpyrrolidone (PVP) as reported in the literature,[30] having a size in the range of 20−30 nm which was expected to

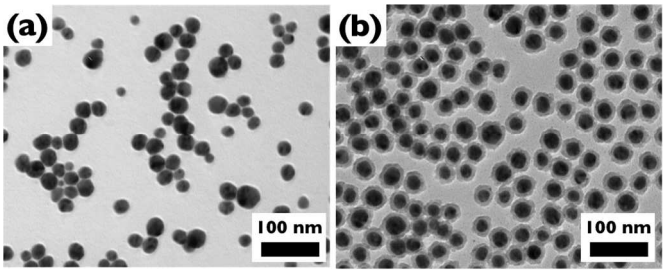

Figure 1. TEM images of (a) Ag NPs and (b) Ag@SiO_2 NPs.

be well introduced in > 100 nm-thick P3HT-PCBM layer and to cause a sufficiently strong scattering effect (Figure 1a). An approximately 10-nm-thick silica shell was coated on the surface of Ag NPs by the controlled hydrolysis/condensation of tetraethyl orthosilicate (TEOS) in ethanol with a base catalyst as reported in the literature (Figure 1b),[31-33] which were expected to optimize the local electromagnetic field near the metal NPs without causing unwanted exciton quenching.[33] The surface of Ag@SiO_2 NPs were modified with (3-trimethoxysilylpropyl)diethylenetriamine (DETAS) having primary and secondary amine groups, as reported to reproducibly generate monolayer coating without using any additional basic catalyst in ethanol,[34] which were then connected to the OT derivative as shown in Scheme 1. The presence of amine groups on the silica layer was simply confirmed by the inversion of surface charges measured by the zeta potential in ethanol (–40 and +48 mV for Ag@SiO_2 and Ag@SiO_2–DETAS NPs, respectively). The pristine surface of silica has negative charges due to the partial deprotonation of Si-OH into Si-O^-, while the surface functionalized with amine groups shows a positive charge owing to the partial protonation of amine groups to form –NH^{3+} and –NH^{2+}–.

Activated OT precursor molecule, 3, was synthesized by the consecutive palladium-catalyzed Suzuki reaction, Vilsmeier-Haack formylation reaction, and Knoevenagel condensation reaction, according to the reported procedures.[35-37] In order to attach the OT derivative to the amine groups on the surface of Ag@SiO_2–DETAS NPs, the terminal carboxyl group of compound 3 was transformed into the activated ester 4 by using N-hydroxysuccinimide with 1-ethyl-3-(3-dimethylaminopropyl)-carbodiimide (EDC). The coupling reaction of Ag@SiO_2–DETAS NPs and activated ester 4 to give Ag@SiO_2–OT NPs, was confirmed by the solubility change of nanoparticles. Ag@SiO_2–DETAS NPs were well dispersed in polar solvents such as ethanol owing to the hydrophilic character of the surface. However, after the modification by OT, the hydrophobic nature of the attached OT groups made the NPs well-dispersed in nonpolar organic solvents such as chloroform and toluene, as shown in Figure 2a. The presence of OT groups on the particles was also confirmed by a thermogravimetric analysis (TGA, see Figure S1). When the temperature was raised from 100 to 800 °C, the weight loss of Ag@SiO_2 NPs was approximately 7 wt%, which could be caused by the elimination of water and decomposition of

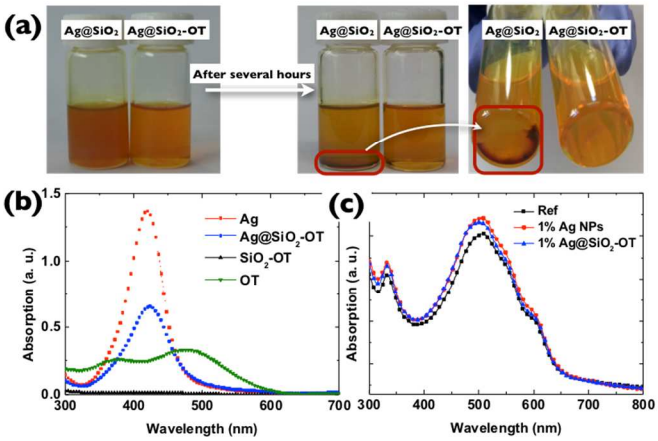

Figure 2. Photograph images of Ag@SiO_2 and Ag@SiO_2–OT in chloroform. (b) Absorption spectra of nanoparticles in 0.001 wt% (w/v) solution and 0.02 mM OT in chloroform and (c) a blended film with P3HT:PCBM = 1:0.8 (w/w).

organic molecules such as the remaining ethoxy group and PVP. TGA analysis of Ag@SiO_2–DETAS also showed very similar weight loss to that of Ag@SiO_2, which is probably due to a relatively small weight portion of DETAS monolayer compared to heavy Ag@SiO_2 particle itself. However, in the case of Ag@SiO_2–OT, the total weight loss increased to 11 % showing 4 % point more weight loss from the attached oligomeric thiophene groups. Based on these TGA data, the number of the attached OT groups on each particle could be calculated (see experimental section). Each Ag@SiO_2–OT particle has ~5,700 OT groups on its silica surface with the packing density value of 0.9 ea/nm^2, which is in the reasonable range of packing density values from quantitative analysis of the surface amine groups using dye absorption (0.44 ea/nm^2) and back-titration (2.7 ea/nm^2) methods,[3,4] because only the primary amine groups can effectively react with a bulky activated ester 4, in our system. Introduced OT groups with the high packing density make the whole particle be well dispersed in nonpolar organic solvent and P3HT:PCBM active layer.

2.2 Photophysical study

UV-Vis absorption spectra of particles (0.001 wt%, w/v) in a chloroform solution and the blended P3HT:PCBM film with either Ag or Ag@SiO_2–OT NPs are presented in Figure 2b and 2c. As shown in Figure 2b, the LSPR peak (λ_{max}) of the Ag NPs was observed with a general extinction characteristic at approximately 420 nm; in contrast, λ_{max} of the Ag@SiO_2 NPs was slightly red-shifted because of the high refractive index of the silica shell around Ag NPs as reported in the literature.[28,38] Compound 4 showed the broad absorption spectrum in the range of 300–600 nm, attributed to the π–π* transition of the conjugated system. However, because most of the mass of SiO_2@OT comes from silica NPs and not from the organic moieties, the absorption intensity of the OT moieties in the SiO_2@OT NPs was almost negligible when the same amount of SiO_2@OT was used as that of compound 4. In other words, OT is more likely to act as a surface ligand rather than as a light-

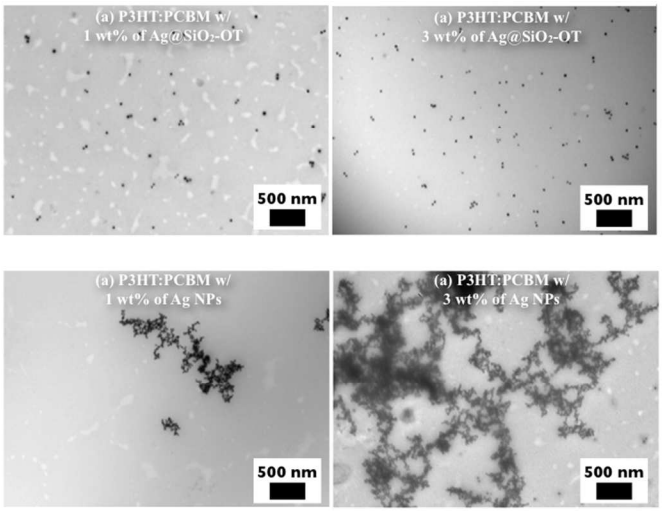

Figure 3. TEM images of composite films of NPs with P3HT:PCBM.

harvesting molecule, because the OT derivatives on the silica surface are much lighter than the silica NPs themselves.

The composite films were prepared by blending a solution of P3HT:PCBM with NPs at 1 wt% (w/w) ratios, fabricated by a spin-casting method, and followed by thermal annealing at 140 °C for 10 min. All samples showed a broad absorption in the wavelength range of 350−650 nm as shown in Figure 2c, where P3HT absorbed characteristically in 400−650 nm region and PCBM at <400 nm. The absorption spectra of the composite films indicated that the light-harvesting ability in the spectral range of 350−600 nm was improved when either Ag or Ag@SiO_2–OT NPs were added to the P3HT:PCBM matrix, compared with that of the film composed only of P3HT:PCBM.

2.3 Morphology studies

Figure 3 shows the TEM images of the various composite films of Ag or Ag@SiO_2–OT NPs with P3HT:PCBM. The individual Ag NPs significantly aggregated during the film casting process, which resulted in the formation of Ag NP aggregates (ca. >1 μm) even when only 1 wt% of Ag NPs were embedded in the active layer (Figure 3c and 3d). In addition, the aggregation was also observed from the composite film of Ag@SiO_2 NPs and P3HT:PCBM film. (see TEM images in Figure S2). On the other hand, as expected for the surface modified Ag@SiO_2–OT NPs, they are well dispersed in the active layer even at 3 wt% (Figure 3a and 3b), demonstrating that surface OT increased the miscibility with P3HT:PCBM to prevent the aggregation of Ag@SiO_2–OT NPs.

The surface morphology of the active layer could affect the photovoltaic performance, which should be closely related with the miscibility of metal NPs and organic components. Figure 4 shows the atomic force microscopy (AFM) images of composite films of P3HT:PCBM with various amounts of NPs. The roughness (R_{rms}) values increased only slightly from 0.548 to 0.635, 0.795, and 0.848 nm as the concentration of Ag@SiO_2–OT NPs increases to 1, 3, and 5 wt%, respectively (Figures 4a, 4b and 4c compared to 4f). These smooth surfaces of composite films of P3HT:PCBM with Ag@SiO_2–OT NPs confirmed again the good miscibility, which would be expected to facilitate the photo-induced charge separation and transport.[27]

In contrast, large aggregates (~200 nm diameter and ~50 nm height) were formed in the composite films of P3HT:PCBM

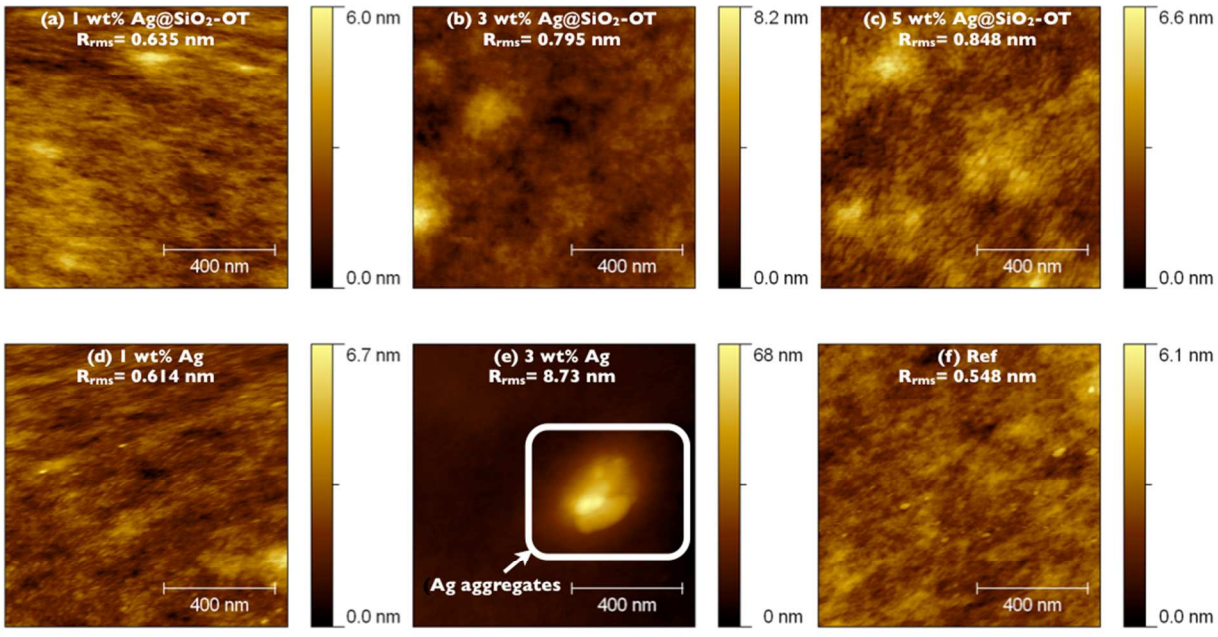

Figure 4. AFM images of composite films of P3HT:PCBM with nanoparticles: (a) 1 wt%, (b) 3 wt%, (c) 5 wt% of Ag@SiO2−OT NPs, (d) 1 wt%, (e) 3 wt% of Ag NPs, and (f) without nanoparticles. Imaging area: 1 μm * 1 μm

Table 1. Photovoltaic performance of representative polymer solar cells with nanoparticles

Types of NPs	NPs ratio		V_{OC} (V)	J_{SC} (mA/cm^2)	FF	PCE (ave.)	PCE (max.)
	NPs (wt%)	Ag content (wt%)					
Ref	0	0	0.62±0.01	10.28±0.41	0.54±0.02	3.44±0.12	3.59
Ag@SiO_2-OT	1	0.66	0.63±0.01	11.42±0.45	0.55±0.01	4.02±0.17	4.25
Ag NPs	1	1	0.63±0.01	11.37±0.35	0.53±0.01	3.78±0.09	3.88

[a]Photovoltaic performance parameters are the average values of at least 10 devices.

with 3 wt% of as-prepared Ag NPs (Figure 4e): the aggregation of Ag NPs could generate charge-trapping sites and defects in the active layer, thus eventually reducing the V_{oc} and device performance as described in the next section.

2.4 Photovoltaic device performance

The photovoltaic devices were fabricated with various composite layers of P3HT:PCBM having different mixing ratios (1–30 wt%) of Ag NPs or Ag@SiO_2–OT NPs. The total concentrations of P3HT:PCBM in chlorobenzene (CB) were kept the same (2 wt%, w/v) in all devices to obtain a uniform, optimized active layer thickness (130–140 nm). The photovoltaic performances and I-V curves of these devices are shown in Table 1, Table S1, and Figure S4. The short-circuit current (J_{sc}) values of the photovoltaic devices having the composite layers of P3HT:PCBM with Ag NPs (11.37 mA/cm^2) or Ag@SiO_2–OT NPs (11.42 mA/cm^2) at 1 wt% (w/w) were higher than those for the devices composed of P3HT:PCBM without NPs (10.28 mA/cm^2). This enhanced photocurrent was confirmed by the incident photon-to-current efficiency (IPCE) spectra. As displayed in Figure S3, the IPCE values for the photovoltaic devices having the composite layers with Ag@SiO_2–OT NPs were higher at all wavelengths than those for the device containing only pristine P3HT:PCBM; the IPCE values stayed higher than 60% in the range from 460 to 560 nm and reached the maximum of 75% at 520 nm. These results support that Ag@SiO_2–OT NPs increase the light-absorption ability due to their LSPR and scattering effects.

For the devices having Ag NPs in the active layer, there was a significant drop in the V_{oc} after incorporating more than 3 wt% of Ag NPs (Figure 5b) in the active layer; similar results have also been reported in the literature.[10, 11] However, in the case of devices fabricated with Ag@SiO_2–OT NPs, the V_{oc} values were perfectly maintained even with a large amount of Ag@SiO_2–OT NPs (up to 30 wt%). This result confirms that the silica shell efficiently inhibits charge trapping on the surface of Ag NPs as expected and direct contact with a metal cathode, which would result in a change in the cathode work function.[26]

Furthermore, not only J_{sc} and FF but also PCE values for the devices having Ag@SiO_2–OT NPs embedded in the active layer were higher than those for the devices having Ag NPs, because the surface-modified NPs formed more uniformly dispersed active layers with low surface roughness values (Figure 4). Especially, the devices having an active layer with 30 wt% Ag@SiO_2–OT NPs showed PCE of 2.65%, while the other with 30 wt% Ag NP showed ohmic contact I-V curve, as shown in Figure S4, which could be attributed to both the aggregation of Ag NPs and the damaged PEDOT:PSS layer caused by a high volume amount of ethanol used to introduce a large amount of Ag NPs.

For the devices having an active layer with Ag NPs, the photovoltaic performances were enhanced for the 1 wt% device but continuously deteriorated as the amount of Ag NPs increased, comparing to the device containing only pristine P3HT:PCBM (Table S2). These phenomena seemed to be consistent with reported results that an initial increase of the exciton generation in the hybrid plasmonic composite OPVs was observed and the high trapping rate of the generated polarons limited the amount of free carriers in the hybrid systems.[40] Thus, as the surface of Ag NPs was modified by introducing SiO_2 layer and oligothiophene derivatives that are structurally similar to P3HT, Ag@SiO_2–OT NPs are efficiently incorporated into the P3HT:PCBM layers without aggregation, resulting in higher enhancement (18%) in the PCE value compared with that of the Ag NP-incorporated device (8%).

2.5 The location of NPs in the active layer

The exact location of Ag@SiO_2–OT NPs within the BHJ layer is a critical issue because the increment of the light-absorption ability due to their LSPR and scattering effects is expected to affect significantly when they are closely located to (photoinduced) electron donor molecules, in this case, P3HT.[40] However, a phase separation within the BHJ layer could not be easily observed in the TEM experiment due to the similar electron densities of both organic components (P3HT and

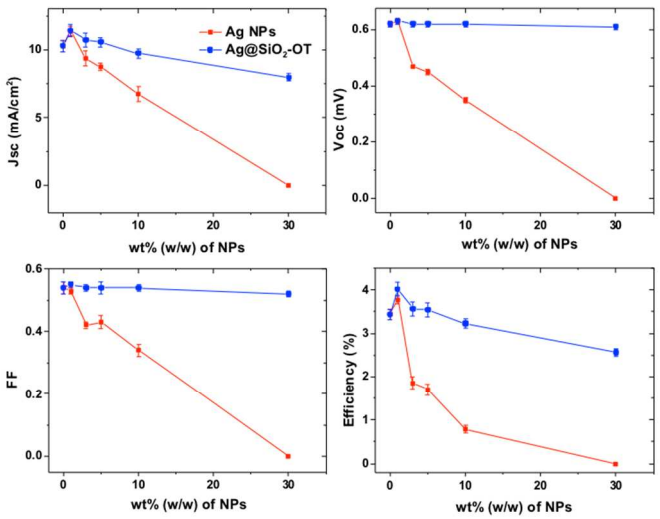

Figure 5. Dependence of the photovoltaic performance of nanoparticle-embedded devices on the concentration of nanoparticles.

PCBM), only showing the existence of Ag@SiO_2–OT NPs within the BHJ layer (Figure 6).

In order to find the exact location of Ag@SiO_2–OT NPs within the BHJ layer, one of the components of the BHJ layer was selectively removed and the differences between the two TEM images were compared. Since 1,8-diiodooctane (DIO) was well-known to dissolve selectively PCBM out of the BHJ layer without affecting P3HT,[41, 42] it was used to remove PCBM from the active layer sample on a TEM grid. The selective removal of PCBM by DIO was also monitored by a decrease in the absorbance of the active layer sample, particularly in the range of shorter than 400 nm (Figure S5), which corresponded to the characteristic absorption band of PCBM.[43] As shown in Figure 6a and 6b, TEM images of the active layer before and after the DIO treatment clearly showed distinguishable dark and bright regions; as the PCBM region was removed by DIO, the darker region corresponded to the stacked P3HT and the brighter region represented the thinner or empty area. The actual location of Ag@SiO_2–OT NPs was also checked using the TEM image of an ultramicrotomed cross section of a sample to show that they were all embedded inside the BHJ layer as shown in Figure 6c. Furthermore, from the results that the majority of NPs was in the dark region and the total number of NPs in the active layer seemed to be maintained after the DIO treatment, it could be concluded that most of Ag@SiO_2–OT NPs were located in the P3HT domain owing to their similar molecular structures of OT and P3HT; which increased the light-absorption ability due to LSPR and scattering effects of NPs and thus affected significantly the efficiency of photo-induced electron transfer (PET) from P3HT to PCBM.

3. Experimental

3.1 Materials and Instruments

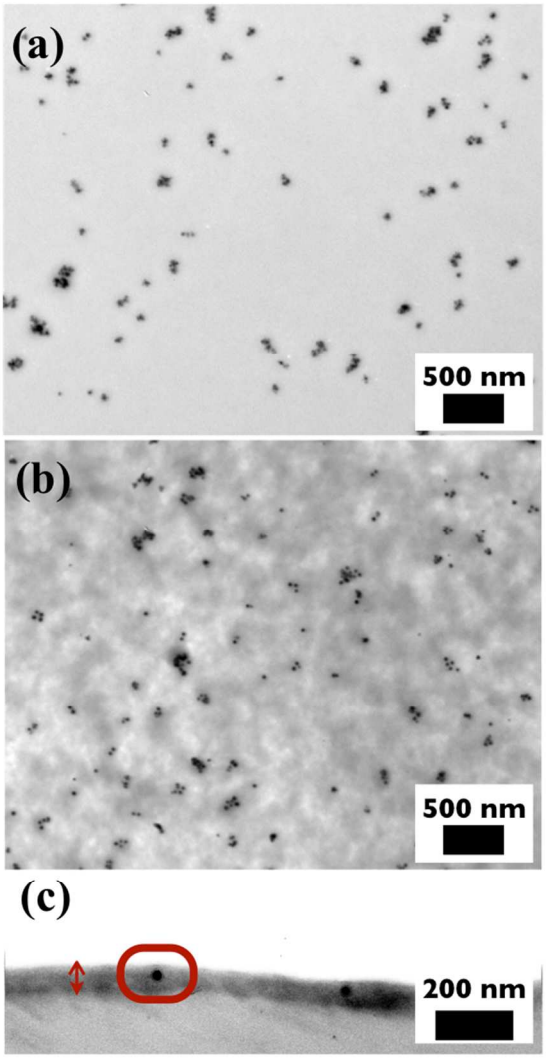

Figure 6. TEM images of blended P3HT:PCBM:Ag@SiO_2–OT = 1:1:0.03 (w/w/w) film (a) before and (b) after DIO treatment. (c) Cross section of film.

All organic chemicals were purchased from Aldrich and TCI. Solar cell materials P3HT and PCBM were purchased from Rieke Metals and Nano-C (USA), respectively. Poly(styrene sulfonate) doped poly(ethylenedioxythiophene) (PEDOT:PSS, Clevious PH) was purchased from Bayer. All solvents and reagents used in this study were commercially available and used without further purification unless otherwise specified. ^{1}H and ^{13}C NMR spectra were recorded using either an Advance 300 MHz Bruker spectrometer or 400 MHz Varian spectrometer. The UV-Vis spectra were recorded using a Beckman DU 650 spec-trophotometer. The mass spectra were obtained using a gas chromatograph-mass spectrometer (JEOL, JMS-AX505WA, HP 5890 Series II). The device performance was measured under AM 1.5G illumination (100 mW cm-2) using a solar simulator (Peccell, Japan) and Solar Cell IPCE Measurement System (McScience, K3100). The light intensity at each wavelength was calibrated using a standard Si solar cell as a reference. Current density-voltage (J-V) curves were measured with a Kethley 2400 source measurement unit. The

TEM images were acquired using Hitachi-7600 (Hitachi, Japan). For cross-sectional TEM images of the active layer, the films were sliced using the MTX ultramicrotome (RMC, USA). The AFM images were obtained using Nanoscope IV controller (Veeco Instruments, USA). Surface charge of NPs was monitored by zeta-potential (Zetasizer nano ZS90, Malvern). The thermo-gravimetric analysis (TGA) was performed using SDT Q600 (TA Instruments Inc.). The TGA samples were preheated at 100 °C for 30 min and then the temperature was raised to 800 °C at 10 °C/min in nitrogen. The active layer thickness was measured using Dektak XT stylus profiler (Bruker, USA).

3.2 Synthesis and characterization

Synthesis of Ag nanoparticles

First, 10 g of polyvinylpyrrolidone (PVP; 10,000 g/mol; TCI) was dissolved in 50 mL of ethylene glycol (EG; Samchun). Then, the reaction temperature was increased to 120 °C. Next, 0.8 g of $AgNO_3$ (Aldrich) was dissolved in 5 mL of EG, and the mixture was added to the PVP solution. After 2 h, the brownish dark product was purified by centrifugation to remove the excess PVP (once at 4,000 rpm for 10 min in acetone, and thrice at 17,000 rpm for 10 min in ethanol), and the final Ag NPs were dispersed in ethanol.

Synthesis of Ag@SiO_2 nanoparticles

First, 120 mg of Ag NPs was dispersed in 120 mL of ethanol. Then, 0.5 mL of tetraethyl orthosilicate (TEOS; TCI) was added to the Ag NP solution, after which 2.5 mL of ammonia solution (29 %; Samchun) and 2.5 mL of water were added. After 6 h, the product was purified by centrifugation (thrice at 17,000 rpm for 10 min in ethanol), and the final NPs were dispersed in ethanol. All processes were performed at room temperature.

Synthesis of SiO_2 nanoparticles

First, 2 mL of TEOS was dissolved in 118 mL of ethanol, and 2.5 mL of ammonia solution and an equal volume of water were added. After the over-night reaction, the product was purified by centrifugation (20,000 rpm, 10 min), and the final NPs were dispersed in ethanol. All processes were performed at room temperature.

Surface modification of nanoparticles with amino-silane group.

First, 0.1 wt% of 3-trimethoxysilylpropyl)diethylenetriamine (DETAS; Gelest) was added to 3 mg/mL ethanol solution of NPs (silica-coated Ag NPs or silica NPs). After 6 h, the product was purified by centrifugation (thrice at 17,000 rpm for 10 min in ethanol), and the final NPs were dispersed in ethanol. All processes were performed at room temperature.

Surface modification of nanoparticles with oligothiophene group

First, 0.1 wt% of a pre-synthesized oligothiophene derivative in chloroform was added to 3 mg/mL ethanol:chloroform (1:1 v/v) mixed solution of NPs (Ag@SiO_2–DETAS or SiO_2–DETAS). After 6 h, the product was purified by centrifugation (once at 17,000 rpm for 10 min in ethanol, and twice at 17,000 rpm for 10 min in chloroform), and the final NPs were dispersed in chloroform. All processes were performed at room temperature.

Simple calculation of the number of attached OT group

When 120 mg of Ag NPs were coated with SiO_2, about 180 mg of Ag@SiO_2 was obtained. It means the weight ratio of Ag:SiO_2 is 2:1 (density of Ag = 10.49 g/cm^2 , SiO_2 = 2.2 g/cm^2). Assuming Ag@SiO_2 has a perfect spherical core@shell structure, the diameter of Ag and thickness of SiO_2 could be approximated to 30 nm and 10 nm, respectively, from the weight ratio and TEM size. Using calculated size and thickness, the amount of OT in Ag@SiO_2–OT from TGA (4 %), and the molecular weight of OT (828.32 g/mol), other parameters in the following table could be calculated (See Table S1).

Device fabrication

Indium tin oxide (ITO)-coated glass, which was cleaned by ultrasonication with detergent, followed by distilled water and 2-propanol sequentially, was used as a transparent electrode. The ITO surface was modified by spin-coating of a 40-nm-thick PEDOT:PSS layer after exposing the ITO surface to ozone for 10 min. The PEDOT:PSS layer was dried on a hot plate in air for 20 min at 140 °C. The reference solution consists of 20 mg/mL (2 wt%, w/v) of P3HT and PCBM (1:0.8, w/w) in CB. To prepare the hybrid solutions, NPs were added to the reference solution at various ratios (1–30 wt%, w/w). The active layer was spin-coated from these solutions over the dried PEDOT:PSS layer at room temperature. The active layer was heated on a hot plate for 10 min at 140 °C. After drying the active layer, LiF (1 nm) and Al metal (100 nm) were deposited as the cathode under vacuum below 10^{-6} Torr, which yielded an active area of 4 mm^2 per pixel. Photovoltaic performance of all devices was investigated at one sun intensity (100 mW cm^{-2}) under simulated AM 1.5G illumination.

For the TEM images of the microtomed samples, the PEDOT:PSS layer was prepared on glass, and an active layer with 3 wt% (w/w) Ag@SiO_2–OT NPs was prepared on the PEDOT:PSS layer. After the entire layer was well dried, only the active layer with the Ag@SiO_2–OT NPs was obtained from the floating film on the water, because the PEDOT:PSS layer was dissolved out by water. Then, the floating film was introduced in an epoxy resin and sliced by an ultramicrotome.

4. Conclusions

In this work, we synthesized silver/silica core-shell NPs and deliberately modified their surface with OT in order to in-crease the light-harvesting ability in polymer solar cells. As the molecular structure of OT on the surface of Ag@SiO_2 NPs is similar to that of P3HT, the Ag@SiO_2–OT NPs are well dispersed in the organic solvents of processing and formed homogeneous composite layers of P3HT:PCBM with various mixing ratios. Furthermore, as the silica shell on the surface of

the Ag NPs protected them from the direct contact with organic materials such as P3HT and PCBM, it efficiently eliminated the trapping problem of initially generated polarons which caused serious limitation for the devices having an active layer with Ag NPs. The performance of the photovoltaic devices based on P3HT:PCBM:Ag@SiO_2–OT = 1:0.8:0.01 (w/w/w) showed nearly 12 % enhancement in the J_{sc} values compared with the pristine P3HT:PCBM device as well as the perfectly maintained V_{oc} values even with 30 wt% NPs, confirming the perfect miscibility of Ag@SiO_2–OT NPs with the P3HT:PCBM layer. Therefore, as the surface of Ag NPs was modified by introducing SiO_2 layer and oligothiophene derivatives, the resulting Ag@SiO_2–OT NPs became miscible with the P3HT:PCBM layer without aggregation, resulting in high enhancement (18%) in the PCE values compared with the pristine P3HT:PCBM device. The TEM images of the active layer of P3HT:PCBM:Ag@SiO_2–OT in which PCBM was selectively washed with DIO solvent revealed that Ag@SiO_2–OT NPs were mainly located in the P3HT domain of the active layer because of the structural similarity between OT and P3HT. Further studies on the modification of the silica surface of metal NPs of different shapes and sizes with various organic molecules for efficient organic solar cells are underway.

Acknowledgements

W. Lee and J. Lim contributed equally to this work. This research was supported by the Pioneer Research Center Program through the National Research Foundation (NRF) of Korea funded by the Ministry of Science, ICT & Future Planning (MSIP, 2012-0009552). This work was also supported by the NRF grant funded by the MSIP for the Center for Next Generation Dye-sensitized Solar Cells (No. 2008-0061903), and by a grant from the New & Renewable Energy Technology Development Program of the KETEP (No. 20113020010070), funded by the Ministry of Knowledge Economy. We thank Dr. Eric Arifin for valuable discussion and comments for the synthesis of Ag nanoparticles. J. Lim is grateful for the award of a BK21 fellowship.

Notes and references

Department of Chemistry, Seoul National University, 1 Gwanak-ro, Gwanak-gu, Seoul, 151-747, Korea

† Footnotes should appear here. These might include comments relevant to but not central to the matter under discussion, limited experimental and spectral data, and crystallographic data.

Electronic Supplementary Information (ESI) available. See DOI: 10.1039/b000000x/

5. References

1 Li, Y., *Acc. Chem. Res.* 2012, **45**, 723.
2 Seo, J. H.; Gutacker, A.; Sun, Y.; Wu, H.; Huang, F.; Cao, Y.; Scherf, U.; Heeger, A. J.; Bazan, G. C., *J. Am. Chem. Soc.* 2011, **133**, 8416-8419.
3 Li, G.; Zhu, R.; Yang, Y., *Nat. Photon.* 2012, **6**, 153.
4 Liang, Y.; Xu, Z.; Xia, J.; Tsai, S. T.; Wu, Y.; Li, G.; Ray, C.; Yu, L., *Adv. Mater.* 2010, **22**, E135.
5 He, Z.; Zhong, C.; Su, S.; Xu, M.; Wu, H.; Cao, Y., *Nat. Photon.* 2012, **6**, 591.
6 Mishra, A.; Bauerle, P., *Angew. Chem. Int. Ed.* 2012, **51**, 2020.
7 Shaw, P. E.; Ruseckas, A.; Samuel, I. D. W., *Adv. Mater.* 2008, **20**, 3516.
8 Goesmann, H.; Feldmann, C., *Angew. Chem. Int. Ed.* 2010, **49**, 1362.
9 Atwater, H. A.; Polman, A., *Nat. Mater.* 2010, **9,** 205.
10 Wang, D. H.; Park, K. H.; Seo, J. H.; Seifter, J.; Jeon, J. H.; Kim, J. K.; Park, J. H.; Park, O. O.; Heeger, A. J., *Adv. Energy Mater.* 2011, **1**, 766.
11 Chen, H. C.; Chou, S. W.; Tseng, W. H.; Chen, I. W. P.; Liu, C. C.; Liu, C.; Liu, C. L.; Chen, C. H.; Wu, C. I.; Chou, P. T., *Adv. Funct. Mater.* 2012, **22,** 3975.
12 Wang, D. H.; Kim do, Y.; Choi, K. W.; Seo, J. H.; Im, S. H.; Park, J. H.; Park, O. O.; Heeger, A. J., *Angew. Chem. Int. Ed.* 2011, **50**, 5519.
13 Xie, F.-X.; Choy, W. C. H.; Wang, C. C. D.; Sha, W. E. I.; Fung, D. D. S., *Appl. Phys. Lett.* 2011, **99**, 153304.
14 Daniel, M.-C.; Astruc, D., *Chem. Rev.* 2003, **104**, 293.
15 Rycenga, M.; Cobley, C. M.; Zeng, J.; Li, W.; Moran, C. H.; Zhang, Q.; Qin, D.; Xia, Y., *Chem. Rev.* 2011, **111,** 3669.
16 Kim, C. H.; Cha, S. H.; Kim, S. C.; Song, M.; Lee, J.; Shin, W. S.; Moon, S. J.; Bahng, J. H.; Kotov, N. A.; Jin, S. H., *ACS Nano* 2011, **5,** 3319.
17 Li, X. H.; Choy, W. C. H.; Lu, H. F.; Sha, W. E. I.; Ho, A. H. P., *Adv. Funct. Mater.* 2013, **23,** 2728.
18 Noh, H. S.; Cho, E. H.; Kim, H. M.; Han, Y. D.; Joo, J., *Org. Electron.* 2013, **14,** 278.
19 Gan, Q.; Bartoli, F. J.; Kafafi, Z. H., *Adv Mater* 2013, **25**, 2385-2396.
20 Wu, J. L.; Chen, F. C.; Hsiao, Y. S.; Chien, F. C.; Chen, P.; Kuo, C. H.; Huang, M. H.; Hsu, C. S., *ACS Nano* 2011, **5**, 959.
21 Chen, F.-C.; Wu, J.-L.; Lee, C.-L.; Hong, Y.; Kuo, C.-H.; Huang, M. H., *Appl. Phys. Lett.* 2009, **95,** 013305.
22 Feng, Q.; Lu, X.; Zhou, G.; Wang, Z.-S., *PCCP* 2012, *14*, 7993.
23 Salvador, M.; MacLeod, B. A.; Hess, A.; Kulkarni, A. P.; Munechika, K.; Chen, J. I.; Ginger, D. S., *ACS Nano* 2012, **6**, 10024.
24 Xue, M.; Li, L.; de Villers, B. J. T.; Shen, H.; Zhu, J.; Yu, Z.; Stieg, A. Z.; Pei, Q.; Schwartz, B. J.; Wang, K. L., *Appl. Phys. Lett.* 2011, **98**, 253302.
25 Topp, K.; Borchert, H.; Johnen, F.; Tunc, A. V.; Knipper, M.; von Hauff, E.; Parisi, J.; Al-Shamery, K., *The J. Phys. Chem. A* 2009, **114,** 3981.
26 Kim, K.; Carroll, D. L., *Appl. Phys. Lett.* 2005, *87*, 203113.
27 Jankovic, V.; Yang, Y. M.; You, J.; Dou, L.; Liu, Y.; Cheung, P.; Chang, J. P.; Yang, Y., *ACS Nano* 2013, **7**, 3815.
28 Choi, H.; Lee, J. P.; Ko, S. J.; Jung, J. W.; Park, H.; Yoo, S.; Park, O.; Jeong, J. R.; Park, S.; Kim, J. Y., *Nano Lett* 2013, **13**, 2204.
29 Xu, X.; Kyaw, A. K. K.; Peng, B.; Zhao, D.; Wong, T. K. S.; Xiong, Q.; Sun, X. W.; Heeger, A. J., *Org. Electron.* 2013, **14**, 2360.
30 Silvert, P.-Y.; Herrera-Urbina, R.; Duvauchelle, N.; Vijayakrishnan, V.; Elhsissen, K. T., *J. Mater. Chem.* 1996, **6,** 573.

31 Arifin, E.; Lee, J.-K., *Bull. Korean Chem. Soc.* 2013, **34**, 539.
32 Yang, J.; Zhang, F.; Chen, Y.; Qian, S.; Hu, P.; Li, W.; Deng, Y.; Fang, Y.; Han, L.; Luqman, M.; Zhao, D., *Chem. Commun.* 2011, **47**, 11618.
33 Graf, C.; Vossen, D. L. J.; Imhof, A.; van Blaaderen, A., *Langmuir* 2003, **19**, 6693.
34 Jung, H.-S.; Moon, D.-S.; Lee, J.-K., *J. Nanomater.* 2012, **2012**, 8.
35 Li, Z.; He, G. R.; Wan, X. J.; Liu, Y. S.; Zhou, J. Y.; Long, G. K.; Zuo, Y.; Zhang, M. T.; Chen, Y. S., *Adv. Energy Mater.* 2012, **2**, 74.
36 Lee, W.; Cho, N.; Kwon, J.; Ko, J.; Hong, J.-I., *Chem. Asian J.* 2012, **7,** 343.
37 Liu, Y.; Zhou, J.; Wan, X.; Chen, Y., *Tetrahedron* 2009, *65*, 5209.
38 Jain, P. K.; El-Sayed, M. A., *Nano Lett.* 2008, **8**, 4347.
39 Dang, M. T.; Hirsch, L.; Wantz, G.; Wuest, J. D., *Chem. Rev.* 2013, **113**, 3734.
40 Wu, B.; Wu, X.; Guan, C.; Fai Tai, K.; Yeow, E. K. L.; Jin Fan, H.; Mathews, N.; Sum, T. C., *Nat. Commun.* 2013, **4,** 2004.
41 Gu, Y.; Wang, C.; Russell, T. P., *Adv. Energy Mater.* 2012, **2**, 683.
42 Lee, J. K.; Ma, W. L.; Brabec, C. J.; Yuen, J.; Moon, J. S.; Kim, J. Y.; Lee, K.; Bazan, G. C.; Heeger, A. J., *J. Am. Chem. Soc.* 2008, **130**, 3619.
43 Cook, S.; Ohkita, H.; Kim, Y.; Benson-Smith, J. J.; Bradley, D. D. C.; Durrant, J. R., *Chem. Phys. Lett.* 2007, **445**, 276.